



A geometrical method for computing the constant-orientation workspace of 6-PRRS parallel manipulators

Ilian A. Bonev, Jaha Ryu *

Department of Mechatronics, Kwangju Institute of Science and Technology, 1 Oryong-dong, Buk-ku, Kwangju 500-712, South Korea

Received 23 June 1999; accepted 29 September 1999

Abstract

This paper presents a geometrical method for the workspace analysis of 6-PRRS parallel manipulators. A geometric algorithm is described for the computation of the constant-orientation workspace, which was implemented in the CAD/CAM system CATIA. The influence of the different design parameters on the workspace, as well as on other properties of the manipulator, is discussed. In addition, a new representation of the mobile platform orientation is presented for easier interpretation of the orientation. Finally, examples are provided to demonstrate the usefulness of the method. © 2000 Elsevier Science Ltd. All rights reserved.

1. Introduction

A 6-DOF fully parallel manipulator, also called a *hexapod*, consists of a *mobile platform* connected by six *legs* to a *base* through, respectively, spherical and universal joints. Most commonly, the base joints are fixed on the base while the legs are of variable length [1,2]. This typical design with six RRPS serial kinematic chains, present in most existing hexapods, will be referred to as the *General Parallel Manipulator* (GPM).

Another common design of 6-DOF parallel manipulators uses six kinematic chains of type PRRS (Fig. 1). In this notation, P stands for an actuated prismatic joint whose axis will be called the *rail axis*, denoted by $A_{i,0}A_{i,1}$, RR for a passive universal joint whose center is denoted by A_i , and S stands for a passive spherical joint whose center is denoted by B_i , where $i = 1, 2, \dots, 6$. In

* Corresponding author. Present address: Departement de Genie Mecanique, University of Laval, Que., Canada, G1K 7P4. Tel.: +82-62-970-2389; fax: +82-62-970-2384.

E-mail addresses: ryu@kjist.ac.kr (J. Ryu), bonev@gmc.ulaval.ca (I.A. Bonev).

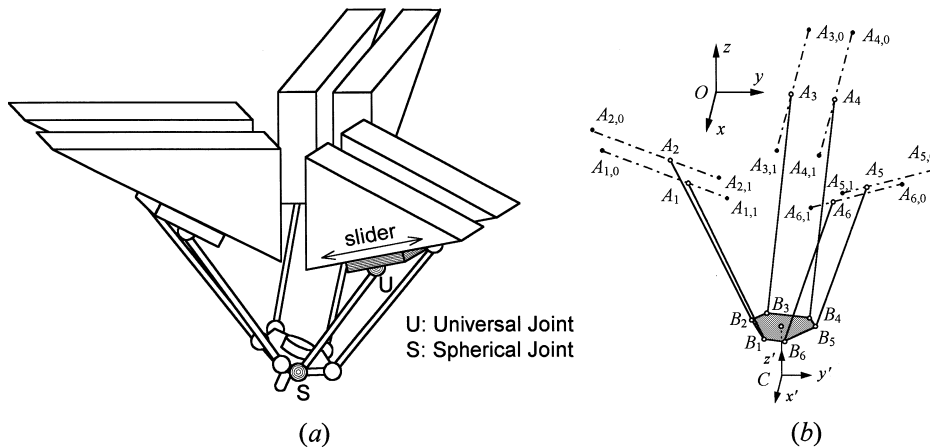


Fig. 1. An example of (a) an HSM and (b) the notation used.

addition, points O and C are, respectively, the centers of the fixed base frame and of the mobile frame. For brevity, we will refer to this type of manipulator as the *HexaSlide Manipulator (HSM)*. Examples of HSMs are the “active wrist” designed by Merlet and Gosselin [3], the “Hexaglide” built at ETH Zurich, the “NPM” proposed by Arai et al. [4], and the commercially available “HexaM” machine by Toyoda.

The main advantages of the HSM over the GPM come from the fact that its actuators are fixed to the base. Each leg is a low-diameter rod of constant length, attached at one end to the actuator tip and at the other to the mobile platform. As a consequence, the HSM exhibits lighter moving mass and reduced risk of leg collision. The drawbacks are a smaller workspace and a need for more complicated analyses because of the more complicated relationship between the mobile platform posture and the actuator lengths.

In the design of parallel manipulators, much concern is given to the workspace factor. As the complete workspace of an HSM is in a six-dimensional space for which no human representation exists, different types of subsets of the complete workspace are usually determined. The most commonly determined workspace is the *constant-orientation workspace*, which is the three-dimensional volume that can be attained by point C when the mobile platform is kept at a constant orientation.

A simple way of determining the workspace of a parallel manipulator is to use a discretization method [1,4–6]. Typically, the workspace boundary is determined in a spherical coordinate system by discretizing the range of azimuth and zenith angles. For each pair of them, the ray radius is augmented until one of the constraint equations is violated, which is checked by solving the inverse kinematics problem. Such a method can be easily applied to any type of robot architecture for any set of mechanical constraints. However, it is computationally intensive and gives little information about the exact boundary of the workspace.

A more advanced geometric approach was first introduced by Gosselin [7] and then again by Gosselin et al. [8] considering only the limits of the actuators. In the first paper, horizontal cross-sections of the workspace have been determined while, in the second, the workspace edges have been defined directly. The first to extend this geometric approach by considering the limited

ranges of the joints and the risk of leg interference was Merlet [9]. All of these researchers were, however, concerned exclusively with the GPM. Unlike the discretization methods, the geometrical methods are very fast and accurate. Furthermore, they bring insight into the problem and are very useful during the design stage. Unfortunately, compared to the GPM, the HSM presents an increased difficulty in conceiving and implementing such a geometric algorithm due to the different type of kinematic chains.

Thus, the main contribution of this article is to extend the geometrical approach to the case of the HSM. In addition, a particular implementation method is suggested, which allows the integration of the whole design process in the commercially available CAD/CAM system CATIA. Based on the geometrical study of the HSM's workspace, we propose simple guidelines for its design, which illustrates the importance of the geometrical approach.

The organization of this paper is as follows. In Section 2, we describe the geometrical method for the constant-orientation workspace of an HSM. Then, in Section 3, we present in detail the general algorithm used for implementation. Based on the proposed geometrical method, we suggest, in Section 4, simple design guidelines for constructing an HSM with desired workspace characteristics. In Section 5, we apply the method to an existing HSM architecture and propose a new Euler angle orientation representation. Further suggestions for extending the proposed geometrical approach for the computation of other types of workspaces are given in Section 6, and the final Section 7 presents the conclusions.

2. Geometrical study of the workspace

In order to describe a geometrical method for computing the workspace of an HSM, it is necessary to establish geometric models for all the constraints that determine the workspace. The basic idea is to first regard all kinematic chains as independent and then to consider their interdependence.

Thus, for a constant orientation of the mobile platform, let us define the *vertex space* i (the term is shared from [12]) as the volume that can be attained by vertex B_i from chain i , ignoring the constraints imposed by all other kinematic chains. The constraints that determine each vertex space are (i) the leg length, (ii) the serial-chain singularity, (iii) the slider–leg interference, (iv) the ranges of the base and mobile platform joints, and, finally, (v) the actuator stroke. Next, we will investigate all the constraints in order to finally construct the vertex space, assuming that all serial chains are identical.

2.1. Leg length

Let the length of a leg be ℓ . Thus, when point A_i coincides with point $A_{i,0}$, the set of points reachable by B_i is a sphere \mathcal{S}_i of radius ℓ and center $A_{i,0}$.

2.2. Serial-chain singularity

A particular characteristic of the HSM is that its serial chains have a singularity at configurations where a leg ($A_i B_i$) is perpendicular to its corresponding rail axis ($A_{i,0} A_{i,1}$). In this

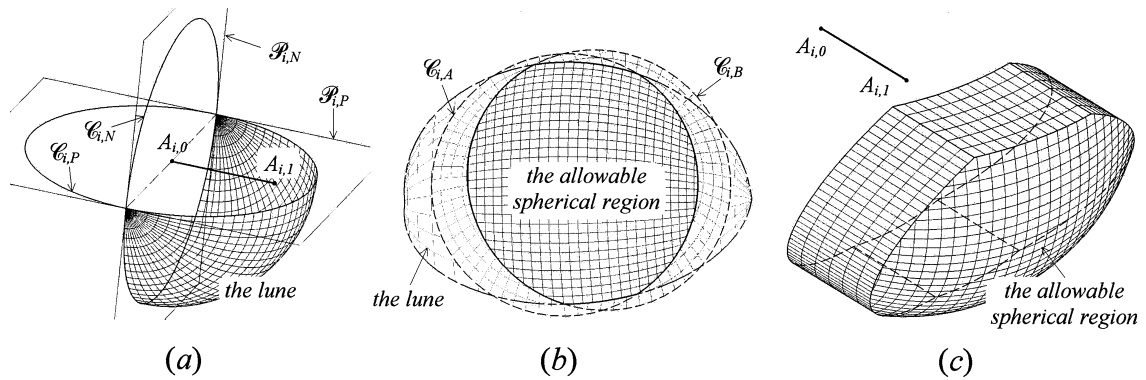


Fig. 2. An example of the vertex space construction: (a) the lune and the elements forming it; (b) the lune and the two spherical caps whose intersection is the allowable spherical region; (c) the final vertex space, obtained by sweeping the allowable spherical region along the directrix $A_{i,0}A_{i,1}$.

singularity, the two branches of the inverse kinematics problem of a chain meet and the mobile platform loses one degree of freedom [10]. Since passing through such a singularity is undesirable, the motion of each leg should be restricted so that the angle between the vectors $\mathbf{A}_i\mathbf{B}_i$ and $\mathbf{A}_{i,0}\mathbf{A}_{i,1}$ is always in only one of the two ranges $[0^\circ, 90^\circ)$ or $(90^\circ, 180^\circ]$. Hence, we split the sphere \mathcal{S}_i by a plane $\mathcal{P}_{i,N}$, normal to the rail axis and passing through point $A_{i,0}$. Without loss of generality, we take only the hemisphere from the side of the rail axis (Fig. 2(a)). The great circle formed by the intersection of \mathcal{S}_i with that plane will be denoted by $\mathcal{C}_{i,N}$.

This constraint has a very peculiar role and, if it is not considered, the workspace analysis changes significantly. At the end of this section, we will discuss what will happen if this constraint is not considered. For the time being, let us just mention that all the existing HSMs are designed to exclude singularities in their serial chains.

2.3. Slider–leg interference

We assume that the prismatic joints are composed of linear motion (LM) guides, which is the case in most existing HSMs. If the actuators are of telescopic type (as in the “active wrist”), then this constraint does not exist and the workspace analysis is simpler. In addition, the workspace is much larger, but the overall stiffness of the manipulator is lower.

The sliders, which move along the LM guides, are relatively wide and with a planar face. To avoid slider–leg collisions, the leg should be only in one of the half-spaces separated by the plane $\mathcal{P}_{i,P}$ parallel to the slider face and passing through point $A_{i,0}$. The great circle formed by the intersection of that plane with \mathcal{S}_i will be denoted by $\mathcal{C}_{i,P}$. Thus, the hemisphere is redefined to a 90° lune (Fig. 2(a)).

2.4. Range of the base joints

The physical constraints that limit the range of a passive joint can be modeled by a general conical surface whose vertex is the center of the joint. We already mentioned that the legs are

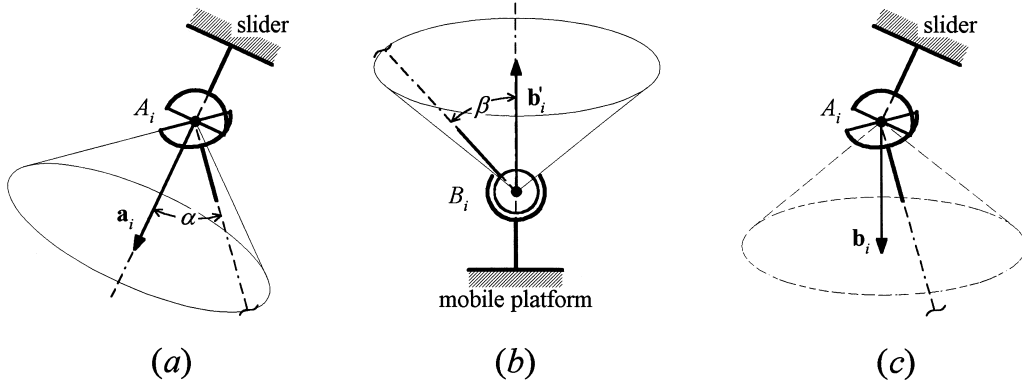


Fig. 3. Mechanical limits on the passive joints: (a) a base universal joint and the cone modeling its range; (b) a platform spherical joint and the cone modeling its range; (c) a base universal joint and the equivalent cone modeling the limitation of the corresponding platform joint at a given orientation.

attached to the sliders through universal joints but, in practice, spherical joints are often used instead. Thus, we choose to model the physical constraint imposed by the base joint as a circular cone (Fig. 3(a)). If, indeed, U-joints were used, then a better model would be a pyramid as used in [9], which, however, will inevitably make the workspace analysis slightly more complicated.

Let α be the maximum misalignment angle of the base joints (assumed to be less than 90°) and let \mathbf{a}_i be the unit vector along the axis of symmetry of the joint at point A_i . Then, the allowable region for point B_i consists of a *spherical cap* of radius ℓ and center A_i . This cap will be denoted by $\mathcal{H}_{i,A}$, and its *base circle* by $\mathcal{C}_{i,A}$ (Fig. 2(b)).

2.5. Range of the mobile platform joints

The same cone model will be used for the platform spherical joints. Let β be the maximum misalignment angle of the platform joints (assumed to be less than 90°) and let \mathbf{b}'_i be the unit vector along the axis of symmetry of the joint with center B_i with respect to the mobile frame (Fig. 3(b)). Then, the allowable region for point A_i , referred to the mobile frame, consists of a spherical cap of radius ℓ and center B_i . Let \mathbf{b}_i be the same unit vector but with opposite direction and with respect to the base frame (Fig. 3(c)), defined as

$$\mathbf{b}_i = -\mathbf{R}\mathbf{b}'_i, \tag{1}$$

where \mathbf{R} is the 3×3 rotation matrix. Thus, with respect to the base frame, the allowable region for point B_i is an identical spherical cap of radius ℓ but center A_i (Fig. 2(b)). This cap will be denoted by $\mathcal{H}_{i,B}$ and its base circle by $\mathcal{C}_{i,B}$.

2.6. Actuator stroke

The *allowable spherical region* for point B_i , when point A_i is fixed, is the intersection of the lune and the two spherical caps defined previously (the square-hatched region in Fig. 2(b)). Now, since point A_i can move between points $A_{i,0}$ and $A_{i,1}$, the allowable spatial region for the vertex B_i is the

volume swept by the allowable spherical region along the directrix $\mathbf{A}_{i,0}\mathbf{A}_{i,1}$. This volume is the vertex space i (Fig. 2(c)).

After the six vertex spaces have been defined, we must consider the fact that all points B_i are rigidly fixed to the mobile platform. Let us call this the *closure constraint*. Since the mobile platform is kept at a constant orientation, the allowable spatial region for point C , taking into account the restrictions imposed by only kinematic chain i , is obtained by translating vertex space i along the vector $\mathbf{B}_i\mathbf{C}$. Thus, the intersection of all six translated vertex spaces is the workspace of the HSM.

Now, to be precise, the next constraints to be considered should be the leg interference and the singularity configurations. Both of these constraints relate to the geometric relationships among the six line segments A_iB_i . For the GPM case, Merlet [9] has shown that the leg interference can be generally modeled by quadratic surfaces, which divide the workspace into separate volumes. Unfortunately, the expressions defining the six line segments A_iB_i of an HSM as functions of the platform orientation are too complicated to involve any algebraic study of these two constraints. Thus, the only way to consider them is by using a numerical method following the application of the geometric algorithm.

Finally, let us see what happens if we do not consider the serial-chain singularity constraint. Instead of a 90° lune, we will have a hemisphere, and the allowable spherical region (recall Fig. 2(b)) may have portions from both sides of the plane $\mathcal{P}_{i,N}$. Sweeping such a spherical surface can only be implemented by sweeping each of its two portions separately and then taking the union of the two swept volumes. Consequently, it may happen that the workspace of the HSM consists of two separate volumes.

3. Implementation algorithms

As we saw, the workspace of an HSM is the intersection of its six translated vertex spaces. Hence, the following two remarks can be made.

Remark 1. The boundary of the workspace consists of portions of spheres, right circular cylinders, elliptic cylinders, and planes.

Remark 2. The edges of the workspace consist of line segments, circular and elliptic arcs, and segments of spatial algebraic curves of order 4.

Next, we will propose a general algorithm for determining each vertex space. The idea is to obtain explicitly the *contour* of the allowable spherical region and then to construct the boundary representation of the vertex space. For simplicity, we assume that $\beta \geq \alpha$.

3.1. Vertex space algorithm

- S1.** If circles $\mathcal{C}_{i,A}$ and $\mathcal{C}_{i,B}$ coincide (i.e., $\alpha = \beta$ and $\mathbf{a}_i = \mathbf{b}_i$), then do not consider $\mathcal{C}_{i,B}$ further.
S2. Calculate the intersection points between all pairs of circles $\mathcal{C}_{i,N}$, $\mathcal{C}_{i,P}$, $\mathcal{C}_{i,A}$, and $\mathcal{C}_{i,B}$, storing each point into lists corresponding to each circle.

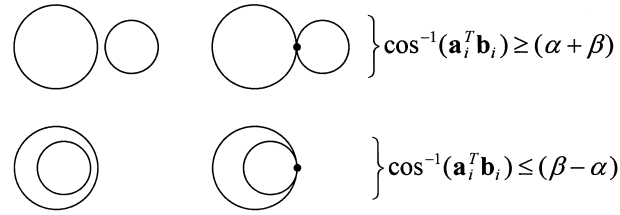


Fig. 4. Schematic representation of the relative locations of the two circles $\mathcal{C}_{i,A}$ (the smaller one) and $\mathcal{C}_{i,B}$ corresponding to 0 or 1 intersection points between them.

S3. For each circle, order its list of intersection points. If two or three points coincide (i.e., three or all of the circles have a common point), then erase all but one.

S4. For each circle, if its list has more than one intersection point, calculate the center point of each arc connecting two successive intersection points. If this center point lies on the lune and on the two spherical caps, then construct the arc and put it into the list defining the contour.

S5. For circles $\mathcal{C}_{i,A}$ and $\mathcal{C}_{i,B}$, if their lists have 0 or 1 intersection points (the cases of which are illustrated in Fig. 4), then check whether $\cos^{-1}(\mathbf{a}_i^T \mathbf{b}_i) \leq (\beta - \alpha)$. If this is not true, then stop (i.e., vertex space i and, consequently, the workspace do not exist for this orientation). Otherwise, put $\mathcal{C}_{i,A}$ in the list and go to step S7 (i.e., the contour is simply the circle $\mathcal{C}_{i,A}$).

S6. Order the list of arcs that define the contour.

S7. Define the spherical patch (i.e., the allowable spherical region) bounded by the contour.

S8. Translate a duplicate of that patch along $\mathbf{A}_{i,0}\mathbf{A}_{i,1}$.

S9. Create the side boundary of the vertex space by offsetting the contour along $\mathbf{A}_{i,0}\mathbf{A}_{i,1}$.

S10. Create a volume from the three boundaries (i.e., the vertex space).

Depending on the available geometry tools and the desired visualization technique, the sequence of steps for constructing the workspace could be different. If no advanced geometry libraries are available, then the horizontal cross-sections of the workspace can be determined as in [9]. Alternatively, the edges of the workspace can be calculated directly as in [8] to obtain a simplified wireframe model. Finally, if a geometric library capable of performing Boolean operations on solids is available, then the workspace can be directly determined in three dimensions as a solid model.

We implemented our approach in the CAD/CAM system CATIA using its IUA application programming interface. This choice was motivated by (i) CATIA's advanced visualization capabilities and (ii) the possibility for integrating the entire design process in one system (synthesis, analysis, and optimization).

4. Design considerations for obtaining a desired workspace

Based on the geometrical description of the workspace, we will now study the design parameters that influence the workspace of the HSM. To allow a systematic study, we will classify the parameters into three groups. The first group consists of the actuator strokes (L), the leg lengths (ℓ), and the ranges of the joints (α, β). The second group includes the arrangement of the LM guides ($\mathbf{OA}_{i,0}, \mathbf{OA}_{i,1}$) and the platform joints (\mathbf{CB}_i). The third group consists of the orientation of

the joints ($\mathbf{a}_i, \mathbf{b}_i$). Finally, we will choose the performance criteria as (i) the volume and (ii) the shape of the workspace at a given orientation, and (iii) their variation as a function of the orientation.

4.1. First group of design parameters

The first group of design parameters relates to the volume and shape of the vertex spaces. The main components of an HSM are the linear actuators or – in the workspace context – their strokes L . Naturally, the larger the stroke, the bigger the workspace.

The next group of components comprises the legs. In general, the longer the legs, the larger the volume of the workspace. When $\ell \gg L$, the volume of the workspace decreases rapidly at greater orientations. When $\ell < L$, the workspace shape becomes slightly simpler. Shorter legs also prevent error amplification.

The last group of components consists of the joints. In order to obtain a maximum vertex space, the lune should be completely covered by the spherical cap $\mathcal{H}_{i,A}$. Thus, for an angle of $\alpha = 90^\circ$, the spherical cap may completely cover the lune, while for an angle of $\alpha \leq 50^\circ$, the spherical cap may cover not more than two thirds of it.

As the orientation of the platform changes, the spherical cap $\mathcal{H}_{i,B}$ covers different regions of the constant intersection of the lune and the cap $\mathcal{H}_{i,A}$. The vertex space will be largest when $\mathcal{H}_{i,B}$ covers that intersection completely. The larger the value of β , the higher the range of orientations at which all the vertex spaces exist.

4.2. Second group of design parameters

The arrangement of the LM guides defines the orientation and initial position of the vertex spaces. This is the most distinguishing characteristic of an HSM, which determines the shape (and volume) of its workspace. For example, if the rail axes are mutually parallel and arranged along a cylindrical surface (as in the “active wrist”), then the workspace is close to a prism. If the rail axes are mutually parallel but coplanar (as in the “Hexaglide”), then the workspace is close to a semicylinder topped with two quarter-spheres.

The arrangement of the LM guides also affects the *resolution* of the HSM. Note that when vertex B_i is close to the cylindrical boundary of the vertex space – i.e., serial chain i is nearly at singular configuration – large actuator displacements lead to small platform motions [11]. In contrast, when vertex B_i is close to the center of the planar boundary of the vertex space – i.e., the leg is almost collinear with the rail axes – the actuator displacements lead to compatible platform motions. Thus, if high resolution is aimed, the rail axes should be arranged in such a way that the resulting boundaries of the workspace be mainly cylindrical (e.g., the “Hexaglide”). Furthermore, the stiffness of such an HSM will be higher since it is less affected by the axial compliance of the LM guides (Fig. 5).

The reasons for the variation of the workspace at different orientations are (i) the variation of the vertex spaces due to the variation of the platform joints’ orientations, and (ii) the variation of the vectors $\mathbf{B}_i\mathbf{C}$. The variation of the workspace is also dependent on the initial arrangement of the LM guides. For the first reason, we already mentioned that increasing the range of the platform joints is the main way to reduce the variation of the vertex spaces. As for the second reason, recall

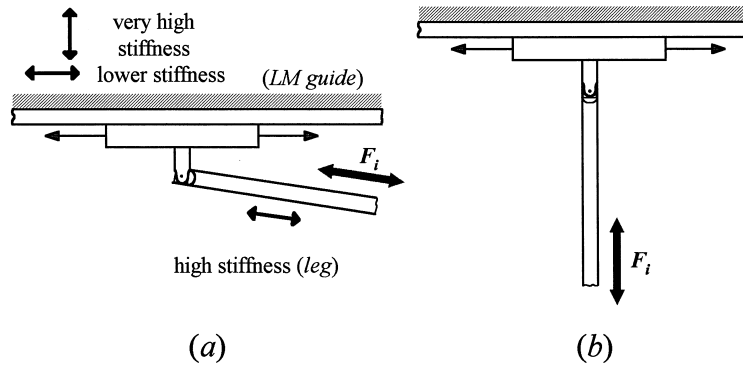


Fig. 5. Two extreme configurations of the serial chains characterized by, respectively, (a) lower and (b) higher stiffness and (a) lower and (b) higher resolution at the end point B_i .

that the arrangement of the platform joints defines the vectors $\mathbf{B}_i\mathbf{C}$ along which the vertex spaces are finally translated. Hence, naturally, the smaller the length of these vectors, the smaller the variation of the workspace. Decreasing the length of these vectors, however, increases the risk of leg interference and decreases the orientational resolution of the mobile platform.

4.3. Third group of design parameters

The final parameters to be considered define the installation of the base and platform joints. Masory and Wang [6] have already suggested how to install the joints of a GPM in order to obtain a larger workspace. A similar guideline is to be followed for the HSM.

For the base joints, we should select each vector \mathbf{a}_i so that it lies in the plane passing through the rail axis and perpendicular to $\mathcal{P}_{i,P}$. In general, the acute angle between a leg and its rail axis is maximum when the mobile platform is in its lowest position and minimum when the platform is in its highest position. Hence, the angle between \mathbf{a}_i and the rail axis should be the average of the maximum and minimum angle. As for the platform joints, the vector \mathbf{b}'_i should be selected in such a way that \mathbf{b}_i is equal to \mathbf{a}_i at the reference orientation since, usually, the workspace at this orientation should be maximum.

5. Example

Before presenting the actual examples, we will introduce briefly a new type of orientation representation using three Euler angles, which was used in the implemented algorithm.

5.1. Orientation representation

Typically, the Euler angles used to represent the orientation of the mobile platform correspond to the angles of three successive rotations about three axes of the mobile or fixed frame. However,

such Euler angles are very difficult to interpret and associate with the corresponding posture of the mobile platform. To overcome this inconvenience, we present a new set of Euler angles.

The three Euler angles (ϕ, θ, ψ) are defined in the following way. First, we rotate the mobile platform about the base z -axis by an angle $-\phi$, then about the base x -axis by an angle θ , then about the base z -axis by an angle ϕ , and finally about the mobile z' -axis by an angle ψ . Defined in this way, angle ψ is the *roll angle*, angle θ is the *tilt angle*, and angle ϕ is the angle between the axis around which the platform is rotated (tilted) and the base x -axis (Fig. 6(a)). The resultant 3×3 rotation matrix \mathbf{R} will be obtained as

$$\mathbf{R} = \mathbf{R}_z(\phi)\mathbf{R}_x(\theta)\mathbf{R}_z(-\phi)\mathbf{R}_{z'}(\psi), \tag{2}$$

where $\mathbf{R}_z(\cdot)$, $\mathbf{R}_x(\cdot)$, $\mathbf{R}_{z'}(\cdot)$ are the basic rotation matrices.

We claim that this representation is a very suitable one for the typical applications of hexapods where axisymmetric tools are used and the user is interested only in the orientation of the tool axis, i.e., in ϕ and θ . First, in this representation, each angle has a clear physical meaning. Second, for a given orientation of the tool axis, we found that the workspace is maximum near or exactly at $\psi = 0^\circ$ (see Fig. 6(b)). Finally, we believe that, at $\psi = 0^\circ$, the risk of leg interference is minimum.

5.2. Workspace of a HexaM type of HSM

To illustrate our geometrical method, we take, as an example, a “HexaM” type of HSM (Fig. 1). In that HSM, $\ell = 900$ mm, $L = 700$ mm, and $\alpha = \beta = 50^\circ$. The LM guides are symmetrically arranged so that points $A_{i,0}$ and $A_{i,1}$ lie on circles with radii of, respectively, 922.301 and 328.467 mm. The rail axes are parallel by pairs. The angle between the rail axes and the horizontal XY -plane is 30° .

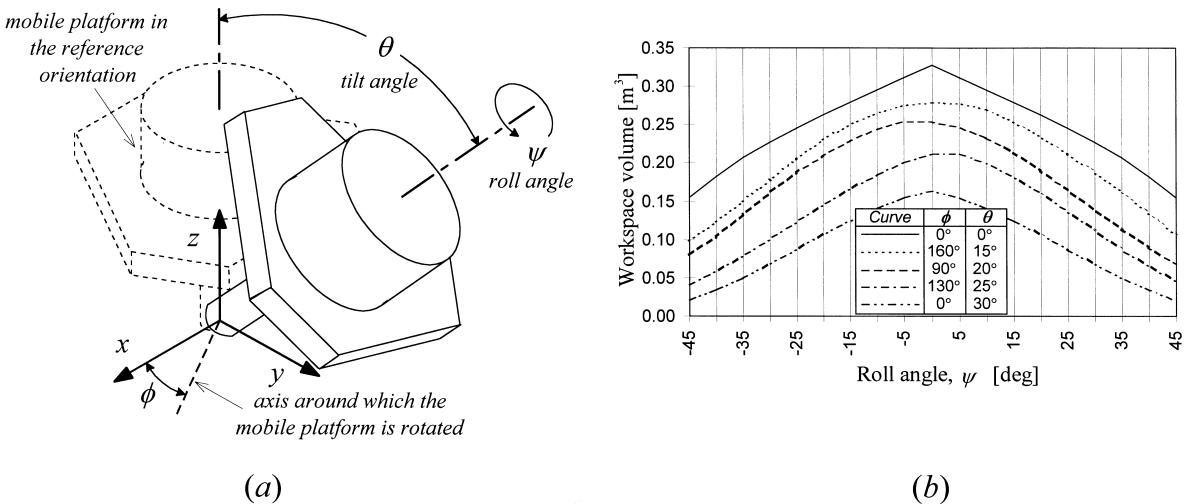


Fig. 6. (a) The three Euler angles defining the orientation of the mobile platform; (b) the volume of the HSM’s workspace as a function of the roll angle ψ for a number of orientations of the tool axis (ϕ, θ) .

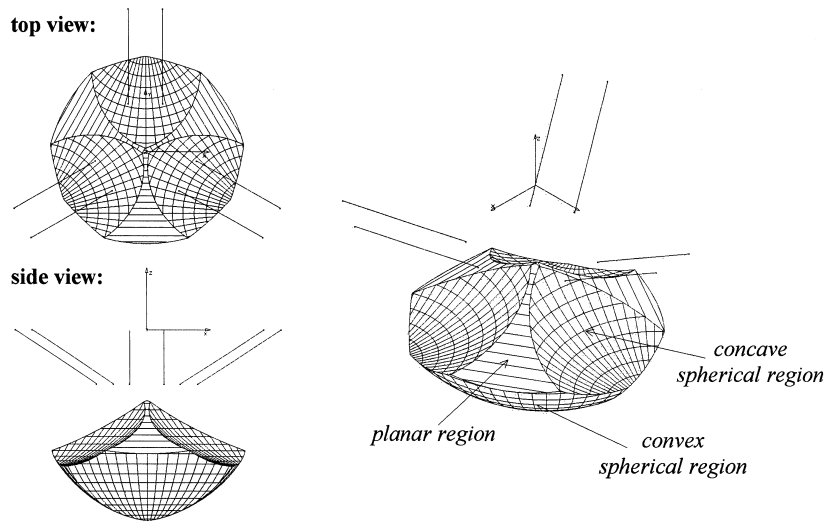


Fig. 7. The workspace of the HSM for the reference orientation. The volume of the workspace is 0.328 m^3 .

We present here two examples of the HSM's workspace. The first one is at the reference orientation (Fig. 7) and the second is at a relatively extreme orientation (Fig. 8). It is interesting to note that the volume of the workspace at the reference orientation (0.328 m^3) is almost equal to the cube of the actuator stroke ($L^3 = 0.343 \text{ m}^3$) and less than one half of the volume of the maximum vertex space (0.720 m^3). Note also its complex shape due to the fact that $\ell > L$. In addition, at this reference orientation, the workspace is not affected by the joint ranges. As for the second example, the workspace is severely limited by the range of one of the platform joints, which accounts for the large portions of elliptic cylinder in the workspace boundary.

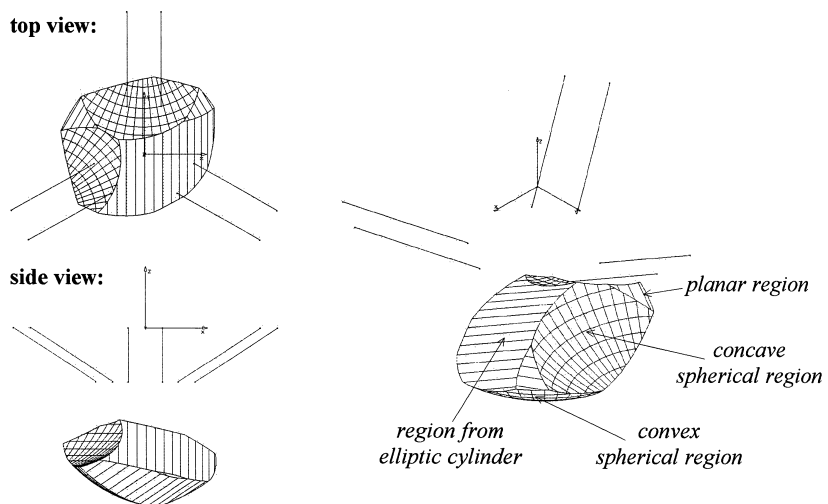


Fig. 8. The workspace of the HSM for $\phi = 25^\circ$, $\theta = 30^\circ$, $\psi = 0^\circ$. The volume of the workspace is 0.151 m^3 .

6. Further suggestions

For some particular HSM designs, some of the rail axes coincide and there is more than one slider moving along the same guideway (e.g. in the “Hexaglide”), which creates a risk of slider–slider collision. In these cases, the proposed geometric method for computing the constant-orientation workspace can be easily extended to consider this slider–slider interference. For a given orientation of the mobile platform, we have to find the locations for point C , for which the distance between points A_i and A_{i+1} , lying on the same rail axis, is equal to some prescribed safety value. For a single pair of sliders, these locations will define a rather simple surface, which will divide the workspace into two separate volumes – one in which there is no interference and one, which is forbidden.

The proposed geometrical approach and the new orientation representation may be extended for determining other types of workspaces. Of great practical interest is the *total orientation workspace* [13] defined as the spatial region in which the mobile platform can reach any orientation within a given range, particularly for $\phi \in [0^\circ, 360^\circ)$, $\theta \in [0^\circ, \theta_{\max}]$, and $\psi = 0^\circ$. For this range, each vertex B_i describes an identical spherical region (close to a spherical cap) with center C . If we neglect the limits on the platform joints, then the six vertex spaces will not be dependent on the orientation of the mobile platform. Therefore, a given point belongs to the total orientation workspace if each spherical region constructed at this point is fully included in the corresponding vertex space.

Finally, the proposed geometrical method can be directly applied to any type of 6-DOF fully parallel manipulator whose base joints A_i are being guided by 1-DOF mechanisms such as circular guides, four-bar linkage mechanisms, etc. In these cases, the allowable spherical region will have to be swept along the trajectory curve of the 1-DOF driving mechanisms, which, in the case of the HSM, is simply a line segment. Clearly, however, the implementation in cases where these curves are more involved will be much more difficult.

7. Conclusions

A geometric algorithm for the determination of the constant-orientation workspace of 6-PRRS parallel manipulators was introduced. The algorithm was implemented in the CAD/CAM system CATIA using its application programming interface. Design considerations were proposed based on the geometric model of the workspace. Finally, an example was presented for the workspace of a HexaM type of manipulator.

It became clear that the frequently mentioned drawback of HSMs over GPMs for having a smaller workspace is compensated by an increased resolution. Combined with its main advantage of having a lighter moving mass, the HSM emerges as indispensable for applications where high accuracy dominates over workspace requirements.

References

- [1] E.F. Fichter, Int. J. Robotics Res. 5 (2) (1986) 157–182.
- [2] K. Liu, J.M. Fitzgerald, F.L. Lewis, IEEE Trans. Ind. Electron. Control Instrum. 40 (2) (1993) 282–293.

- [3] J.-P. Merlet, C.M. Gosselin, *Mech. Mach. Theory* 2 (26) (1991) 77–90.
- [4] T. Arai, T. Tanikawa, J.-P. Merlet, T. Sendai, in: *ASME Japan/USA Symposium on Flexible Automation*, vol. 1, Boston, 1996, pp. 145–149.
- [5] J.P. Conti, C.M. Clinton, G. Zhang, A.J. Wavering, *Technical Research Report 97-28*, ISR, University of Maryland, MD, 1997.
- [6] O. Masory, J. Wang, *ASME 22nd Biennial Mechanisms Conference*, vol. 45, Scottsdale, 1992, pp. 337–346.
- [7] C.M. Gosselin, *J. Mech. Des.* 112 (1990) 331–336.
- [8] C.M. Gosselin, E. Lavoie, P. Toutant, *ASME 22nd Biennial Mechanisms Conference*, vol. 45, Scottsdale, 1992, pp. 323–328.
- [9] J.-P. Merlet, *Mech. Mach. Theory* 29 (8) (1994) 1099–1113.
- [10] C.M. Gosselin, J. Angeles, *IEEE Trans. Robotics Autom.* 6 (3) (1990) 281–290.
- [11] J.A. Carretero, M. Nahon, C.M. Gosselin, B. Buckham, in: *ASME Design Engineering Technical Conference*, Sacramento, California, 1997.
- [12] Z. Ji, *J. Robotic Syst.* 11 (7) (1994) 631–639.
- [13] J.-P. Merlet, C.M. Gosselin, N. Mouly, *Mech. Mach. Theory* 33 (1/2) (1998) 7–20.